The Effects of Ultrasound Parameters and Microbubble Concentration on Acoustic Particle Palpation

This is a post-refereeing final draft. When citing, please refer to the published version: N. Saharkhiz, H. Koruk, J.J Choi, The Effects of Ultrasound Parameters and Microbubble Concentration on Acoustic Particle Palpation, The Journal of the Acoustical Society of America 144(2), 796-805, **2018**. https://doi.org/10.1121/1.5050524

1 2

The Effects of Ultrasound Parameters and Microbubble Concentration on Acoustic Particle Palpation

Niloufar Saharkhiz,[1] Hasan Koruk,[2] and James J. Choi[1, a)]

[1]*Department of Bioengineering, Imperial College London, Exhibition Road, London SW7 2BP, United Kingdom*

[2]*Mechanical Engineering Department, MEF University, Ayazaga Caddesi, No.4, Sariyer, Istanbul 34396, Turkey*

The elasticity of tissue - an indicator of disease progression - can be imaged by ultrasound elasticity imaging technologies. An acoustic particle palpation (APP) has recently been developed - the use of ultrasonically-driven acoustic particles (e.g., microbubbles) - as an alternative method of tissue deformation. APP has the potential to improve the resolution, contrast, and depth of ultrasound elasticity imaging; but the tissue displacement dynamics and its dependence on acoustic pressure, center frequency, and microbubble concentration remains unknown. Here, we produced displacements of at least 1 μm by applying ultrasound onto a microbubble solution (concentration: 10×10^6 microbubbles ml^{-1}) placed within a tunnel surrounded by a 5% gelatin phantom. Displacements of more than 10 μm were produced using a 1, 3.5, or 5 MHz center frequency pulse with peak-rarefactional pressures of 470, 785, and 1,210 kPa, respectively. The deformation of the distal wall varied spatially and temporally according to the different parameters investigated. At low pressures, the deformation increased over several milliseconds until it was held at a nearly constant value. At high pressures, a large deformation occurred within a millisecond followed by a sharp decrease and long stabilization. Ultrasound exposure in the presence of microbubbles produced tissue deformation ($p < 0.05$) while without microbubbles, no deformation was observed.

[a)]j.choi@imperial.ac.uk

I. INTRODUCTION

Changes to the elastic properties of tissue are strong indicators of disease progression. In cancer (**?**), liver cirrhosis (**?**), and other diseases, tissue stiffens over time. Quantifying and imaging changes in elasticity are thus major goals in imaging modalities, such as ultrasound and magnetic resonance imaging (MRI) (**?**). The general steps for measuring elasticity noninvasively using acoustic radiation force (ARF) is to apply the force to the tissue (i.e., palpation), monitor the resulting deformation, and derive the elasticity using a model (**???**). In these techniques, ARF is applied by focusing ultrasound onto a region of excitation (ROE) and is proportional to the intensity of ultrasound and the absorption coefficient of the tissue (**?**). The deformation can be monitored by ultrasound or other modalities, such as MRI and optical imaging. Despite the benefits of ARF-based elasticity imaging, there are diseases, such as micro-metastatic cancers and distal regions of the liver, which cannot be imaged due to poor imaging depth, contrast, or resolution (**?**).

Lipid-shelled and gas-filled microbubbles are routinely used in the clinic as ultrasound contrast agents to improve the quality of ultrasound images (**?**). This contrast enhancement takes advantage of a microbubble's unique behavior in an acoustic field: nonlinear volumetric oscillations that enhance scattering. Ultrasound exposure of a microbubble also generates a primary radiation force (or Bjerknes) force which is proportional to the spatial derivative of the acoustic pressure and the bubble's volume (**?**). Microbubbles undergoing primary radiation force move in the direction of ultrasound propagation (**?**). Microbubbles also experience a secondary radiation force, which is an attractive or repulsive force between

oscillating bubbles. This force becomes relevant as the distance between adjacent bubbles is reduced (i.e., high concentrations) and as the pressure and pulse length increase (**?**).

Bubbles exposed to ultrasound have been previously used to measure the elasticity of viscoelastic media (**?**). In one approach, large bubbles were formed by vaporization of a hydrogel (gelatin) with a laser. This laser-generated bubble had a radii between 18 and 78 μm and was used to measure the Young's modulus of the material. In another study, the elastic properties of materials was measured by exposing a large laser-generated bubble (diameter: 100-800 μm) to an acoustic field (**?**). Moreover, some experiments have been conducted to characterize the time-dependent mechanical properties of microvessels by optically imaging the tissue's response to an ultrasonically-driven microbubble collapse (i.e., inertial cavitation) against vessel walls (**?**).

We recently explored the use of pre-formed microbubbles undergoing primary ARF - acoustic particle palpation (APP) - as a stress source for elasticity imaging (**?**). In this technique, microbubbles were administered into a vessel that modelled the bloodstream of tissue. The application of ultrasound caused the microbubbles to move in the direction of wave propagation and push against the distal vessel wall, resulting in tissue deformation. It was shown that a larger force was applied with APP than with ultrasound only ARF-based methods (**?**). Microbubbles used in this manner are acting as contrast agents for elasticity imaging. However, just as contrast agents for ultrasound imaging are not simply the enhancement of tissue contrast - it is the blood supply that is enhanced - microbubbles in APP would not enhance the tissue contrast directly. Microbubbles are contained within the vasculature and thus the vessel wall would be assessed. Thus, APP-based imaging may be able to probe

large vessels such as arteries or veins. The Young's modulus of arteries in human can range from 0.3 to 5.5 MPa (**?**) with the mass density of 1050-1075 kg m^{-3} (**?**) and the speed of sound of 1560-1660 m s^{-1} (**?**). These properties depend on the composition of the vascular tissue such as collagen, elastin and smooth muscle cells (**?**) and will change with age and the progression of vascular diseases (**??**). However, the vessel's properties in APP-based imaging may be far less relevant as the probed vessels approach the size of arterioles, venules and capillaries. In such small vessels, their thickness approaches a single cell and in the case of microvessels with very thin walls, the vessel takes on the elasticity of the surrounding tissue microstructures (**?**). For soft tissue such as liver, the Young's modulus, mass density and speed of sound are 0.6 kPa (**?**), 1050 kg m^{-3} (**?**) and 1578 m s^{-1} (**?**) respectively. APP techniques are not limited to just vessels and could potentially measure the elastic properties of the other tissue types by injecting the particles into the cerebrospinal fluid, fluid bodies or subcutaneously into the lymphatic system (**?**). Thus, there is a potential for measuring the stiffness of tissue microenvironments. But to make this elasticity measurement technique pragmatic, it must be safe and effective. One of the concerns with sonicated microbubbles is that high magnitudes of inertial cavitation may damage the surrounding tissue environment. This occurs when the rarefactional phase of an ultrasonic pulse is high enough to cause the bubble to unstably expand to at least twice its initial radius (**?**), which leads to a rapid collapse due to the inertia of the surrounding fluid. This phenomenon depends on the frequency of ultrasound, peak rarefactional pressure and pulse length (**?**). As a result, the acoustic parameters must be below a threshold to minimize the magnitude of inertial cavitation. Although there is some debate about when in vivo bio-effects arise, studies

have suggested that the mechanical index (MI) should be kept below 0.4 when ultrasound is applied in the presence of certain types of microbubbles (**?**). The MI is proportional to the peak-rarefactional pressure and inversely proportional to the square root of the center frequency. Since APP can be achieved with very low intensities (low acoustic pressures and short duty cycles), we anticipate very low thermal index (TI) values.

The purpose of this study is to identify a range of ultrasound and microbubble conditions that can generate APP to an extent that is relevant for elasticity imaging. Microbubbles flowing through a wall-less channel in a 5% gelatin phantom was exposed to ultrasound to cause deformation of the distal tissue wall. The Young's modulus of 5% gelatin phantom is approximately 1.5 kPa as determined in previous studies (**??**) and is similar to the elasticity of the brain in young rats (**?**) and liver in humans (**?**). The effects of different center frequencies (1, 3.5, and 5 MHz), which are below, close and above the resonance frequency of microbubbles, were investigated. A wide range of acoustic pressures were applied (peak negative of 0.3 to 2 MPa) to observe how microbubbles behaved below, at, and above the MI threshold for clinical safety. Experiments were also conducted with a range of microbubble concentrations (4×10^6, 10×10^6 and 20×10^6 microbubbles ml^{-1}) to explore the possibility of palpating tissue using low microbubble concentrations.

II. MATERIALS AND METHODS

A. Tissue Mimicking Material

Experiments were conducted with gelatin phantoms that mimicked the elastic and acoustic properties of tissue (**?**). These phantoms had a speed of sound of approximately 1540 m s^{-1}, a mass density of approximately 1 g cm^{-3} and a Young's modulus of approximately $10^0 - 10^2$ kPa (**?**). To prepare each phantom, 10 g of gelatin powder (Fisher Scientific UK Ltd, Loughborough, UK) was added to 200 ml of degassed and deionized water. The solution was dissolved by heating (42 $^{\circ}C$ for 40 minutes), stirred continuously to create a homogenous solution, and then degassed for 30 minutes under the vacuum strength of 720 mmHg in a vacuum chamber. The mixture was poured into a phantom box which had two Mylar sheets that allowed for ultrasound to enter and leave the box. An 800-μm-in-diameter carbon rod (Hyperflight, UK) was inserted into the phantom. The box was then refrigerated overnight (approximately 12 hours) so that the solution solidified. Each phantom was left at room temperature (22 $^{\circ}C$) for an hour prior to experiments. The rod was then removed before sonication to provide a wall-less tunnel for water and microbubbles to flow through.

B. Microbubble Preparation

Lipid-shelled microbubbles were prepared according to a previously described method (**?**). Dipalmitoylphosphatidylcholine (DPPC-82%), Dipalmitoylphosphatidic acid (DPPA-8%), and dipalmitolyphosphatidylethanolamine-PEG5000 (DPPE-PEG5000-10%) (Avanti Polar Lipids Inc., AL, USA) were mixed and diluted with saline and glycerol. Each vial was

filled with perfluorobutane gas (FluoroMed L.P., Texas, USA) and placed in a mechanical shaker (Synergy Electronics, Scottsdale, AZ, USA) for 45 seconds to activate the bubbles. The size and population distribution of the bubbles were calculated by optical microscopy followed by image processing using a previously described technique (**?**). The mean diameter of the bubbles was 2.07 ± 1.28 μm with a range from 0.5 to 9.87 μm. The undiluted vial concentration was 3.83×10^9 microbubbles ml^{-1}; approximately 2000 times the clinical dose of 2.04×10^6 microbubbles ml^{-1}. This clinical dose was based on a 0.02 ml kg^{-1} recommendation while assuming a 5 L blood volume for a 70 kg individual (**?**). Diluted microbubbles solutions were prepared by diluting the vial's content with select amounts of deionized, degassed water for each experiment.

C. Experimental Setup

The tissue-mimicking phantom was placed in a water tank using a 3-D manual positioning system (Newport, Bloomfield, NY, USA). The tank's water was degassed and deionized. A high frame rate camera (frame rate: 1200 frames per second, field of view: 416×144 pixels, model: Nikon 1 V3, Nikon Inc., USA) with an attached lens (Nikon VR 70-300 f/4.5-5.6) was used to record the displacement of the channel (Fig. **??**). Two magnifying glasses with magnification factors of 10x were used to improve the resolution to 10 μm pixel^{-1}. An LED light source (KL 2500 LED, SCOTT, Stafford, UK) with gooseneck guides was used for backlight illumination and to increase the contrast between the wall-less channel and the background (Fig. **??**). For all experiments, microbubbles flowed across the channel using a syringe pump (70-3007, Harvard Apparatus, Cambridge, UK) and plastic tubes (R 3603,

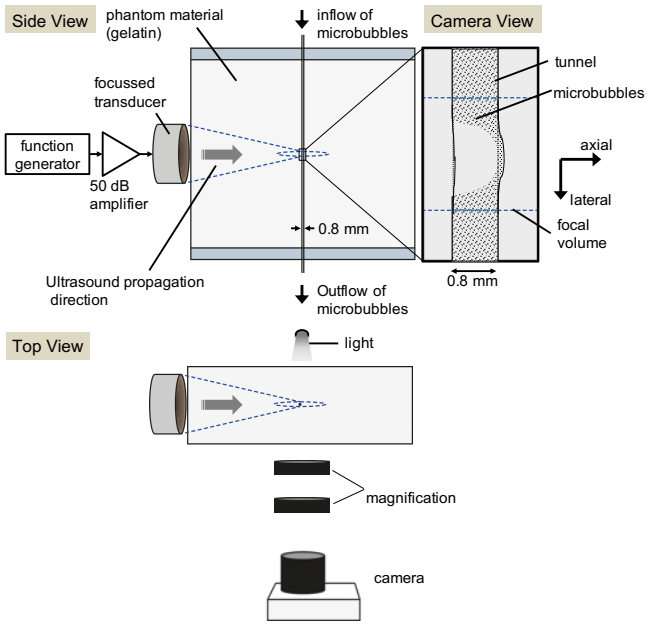

FIG. 1. Experimental setup. A solution of microbubbles flowing through a 0.8 mm wall-less channel were sonicated by a focused ultrasound transducer. The channel was created in a 5% gelatin phantom which was immersed in a water tank. The transducer was driven by a function generator and 50 dB amplifier (side view). The sonicated bubbles applied a force to the channel's wall and deformed it (Camera view). The deformation of the wall was recorded by a high frame rate camera. Two magnifying glasses were used to increase the resolution of the final image. To increase the contrast between the channel and the phantom material, the background was illuminated (top view).

Tygon) attached to the connectors on the phantom box. The flow rate was 700 μl min^{-1} and the velocity was 23 mm s^{-1}.

Three different single element transducers (Power Series, Olympus Industrials, UK) of 1 MHz (aperture diameter: 25.4 mm, f-number: 0.9, FWHM: 4.77 mm, focal length: 51.15 mm, part number:18-0116-P), 3.5 MHz (aperture diameter: 19.05 mm, f-number: 3.3, FWHM:

1.71 mm, focal length: 52.02 mm, part number:17-0312-P) and 5 MHz (aperture diameter: 25.4 mm, f-number: 4.8, FWHM: 0.83 mm, focal length: 52.30 mm, part number:18-0516-P) were used. Each transducer was calibrated in free field by a hydrophone (Precision Acoustics Ltd., Dorchester, UK) in a separate set of experiments. In order to place the transducer's focal volume over the tube, we first imaged the rod that remained embedded in the phantom. In an imaging configuration, the transducer was connected to a pulser/receiver (DPR300, JSR Ultrasonics, Pittsford, NY, USA) and oscilloscope (DPO3014, Tektronix, Inc. OR, USA) to position the transducer axially. The carbon rod was then gently removed from the phantom. The lateral targeting was conducted by imaging an air bubble that filled the channel after the rod was removed. In the APP configuration, the transducer was driven by a waveform generator (33500B Series, Agilent Technologies, Santa Clara, CA, USA) and 50 dB power amplifier (Precision Acoustics Ltd, Dorchester, UK) to produce a specific range of beam characteristics (Table **??**).

After alignment of the transducer, the control experiment (without the presence of the microbubbles) was conducted by establishing a flow of degassed, deionized water through the channel. The channel was then filled with a flow of diluted microbubbles. The channel was cleaned after each experiment by flowing an air bubble across the channel. In order to evaluate whether residual microbubbles accumulated in the channel, a second control experiment with water was conducted at the end of the experiments. No significant difference in deformation was observed between the initial and final controls. For all experiments, images were captured before, during and after ultrasound excitation (Fig. **??**)

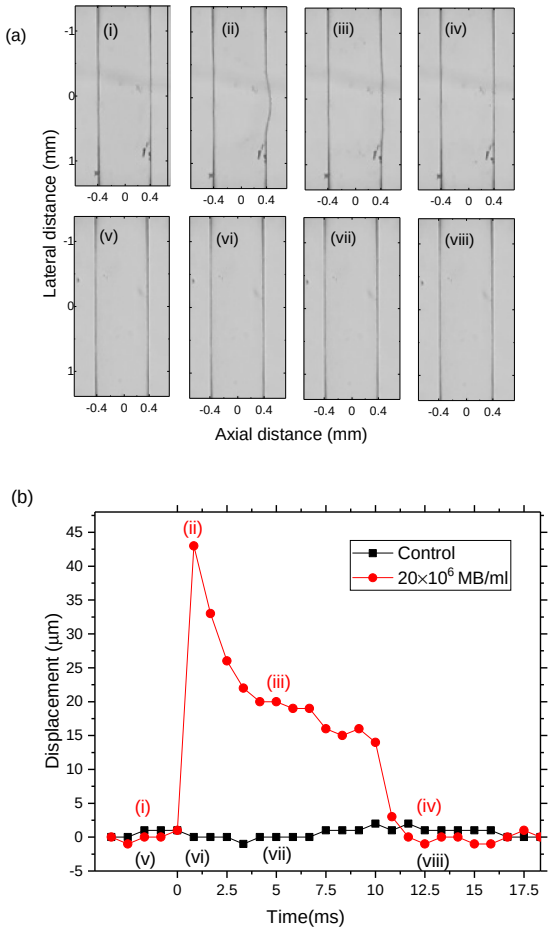

FIG. 2. (a) The images acquired by the camera of the wall less channel pre, during and post excitation (center frequency: 5 MHz, peak-rarefactional pressure: 2210 kPa, pulse length: 10 ms) with the channel filled (i-iv) with the microbubbles and (v-vii) with water alone (Control). The images are captured (i), (v) before the excitation and (ii-iv), (vi-vii) at 0.83, 4.98 and 12.45 ms after the start of the excitation. MB: microbubbles. (b) Displacement over the length of the pulse for the corresponding images.

D. Deformation Analysis

In order to analyze the APP-induced deformation dynamics, we tracked and collected the wall deformation using the pixels from the images captured by the camera and processed with MATLAB (The Mathworks, Natick, MA, USA). Since wall deformation occurred in the direction of wave propagation, we anticipated that the deformation would occur on and orthogonal to the distal wall. Our first step was to automatically detect where the wall was located within each image. This was achieved by tracking a 1-D line of pixels along the axial axis. Once this was found, each image was interpolated by a factor of 10 along the axial dimension. The overlap of the focal volume with the distal wall was detected and the focal center of the ultrasound beam on the distal wall was determined which was assumed as the middle of the previously detected overlapped area. An average of five adjacent pixels in the focal center were considered in our deformation measurements. The displacement of the focal center pixels in each frame was measured using 1-D cross-correlation. The position of the focal center was averaged at five to ten frames before the excitation and was considered as the reference for the cross-correlation algorithm.

E. Statistical Analysis

The mean and standard deviation values were calculated based on the deformation values for five consecutive pulses. Statistical tests, one-way analysis of variance (ANOVA) followed by post-hoc Bonferroni analysis, were performed to check the significance of the results. The data sets for different microbubble solutions at each acoustic pressure for each of the

TABLE I. Ultrasound parameters

Parameters	*Set* 1	*Set* 2	*Set* 3
Frequency (MHz)	1	3.5	5
Peak-negative pressure (kPa)	240 to 734	325 to 1395	325 to 1395
Pulse length (ms)	20	10	10
Pulse repetition period (ms)	200	200	200
Number of pulses	5	5	5

transducers were compared and a P value of 0.05 was considered to determine the significant difference. Linear regression was also performed to compare the displacement amplitudes for different solutions over all the applied acoustic pressures.

III. RESULTS

A. Deformation Dynamics

A uniform flow of microbubbles with a concentration of 20×10^6 microbubbles ml^{-1} was established through the channel before the excitation ((Fig. **??**(a).i), (Fig. **??**(b).i)). The 5 MHz transducer was driven at a peak-rarefactional pressure of 2,210 kPa, which pushed the microbubbles towards the distal wall of the channel and created a large wall displacement of approximately 43 μm ((Fig. **??**(a).ii), (Fig. **??**(b).ii)). The displacement decreased rapidly in the following frames ((Fig. **??**(a).iii), (Fig. **??**(b).iii)). Finally, the channel wall returned

to its initial position after the removal of ultrasound ((Fig. **??**(a).iv), (Fig. **??**(b).iv)). The same experiment was conducted with the channel filled with water and without the presence of the microbubbles. No deformation of the channel was observed in the control experiment ((Fig. **??**(a).v-vii), (Fig. **??**(b).v-vii)).

B. Acoustic Pressure

In order to evaluate the effect of different acoustic pressures on the APP, the 1 MHz transducer was driven at different pressures (peak-rarefactional pressure from 240 to 734 kPa). As expected, higher acoustic pressure produced greater displacements. In one set of experiments with a microbubble concentration of 10×10^6 microbubbles ml^{-1}, it was observed that low pressure exposure (i.e. 470 kPa) produced a displacement of the wall that was nearly constant during the entire pulse duration. Increasing the pressure above 520 kPa (i.e. 734 kPa) led to a displacement up to 14 ± 3.58 μm (0.83 ms after the start of the excitation), which rapidly decreased in the following frames (Fig **??**(a)). In the control experiments at the highest pressure (i.e., 734 kPa), a very small net displacement of 1.86 μ m was observed while no displacement was observed at lower pressures.

We evaluated similar experiments with the 3.5 MHz transducer (Fig. **??**(b)). No displacement was observed in our control where the channel filled with water, was exposed to acoustic pulses at 1,395 kPa. In the presence of microbubbles (concentration: 10×10^6 microbubbles ml^{-1}), ultrasound exposure at 785 and 1395 kPa produced a maximum displacement of 8.8 ± 1.58 μm and 16.2 ± 4.39 μm, respectively. The displacement pattern where an initial peak displacement followed by a decrease in the following frames, was observed for acoustic

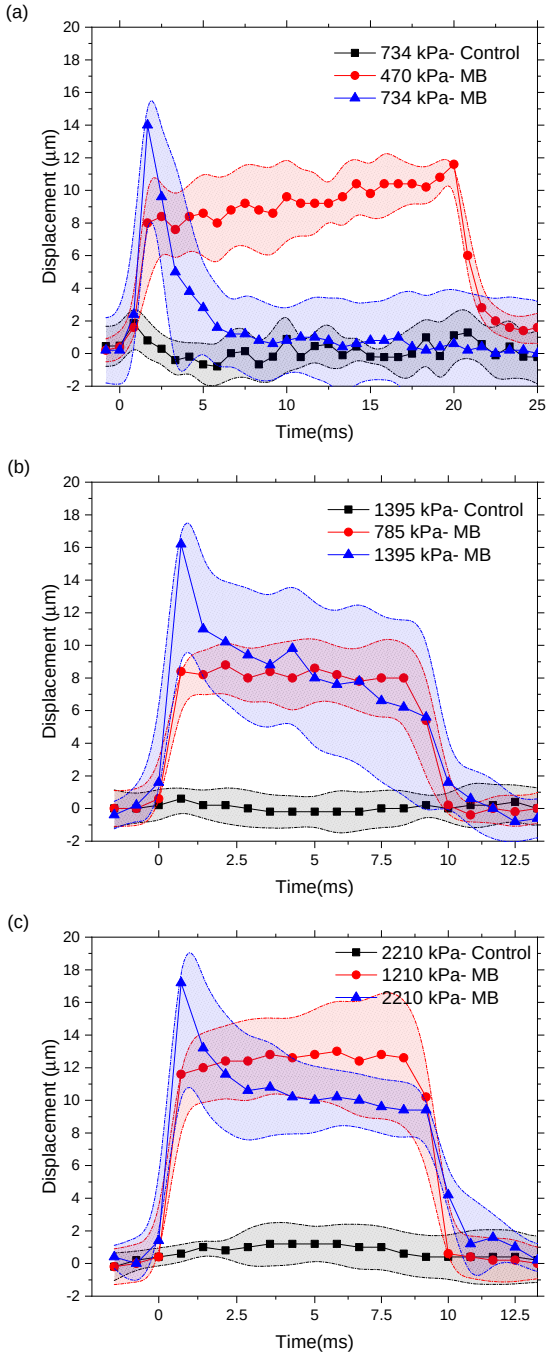

FIG. 3. Displacement over the length of the pulse. The deformation of the distal wall was tracked for different ultrasound exposure conditions (circles and triangles) with and (squares) without microbubbles. Displacements are shown as averages for five consecutive pulses using (a) 1 MHz, (b) 3.5 MHz, and (c) 5 MHz transducer. The microbubble (MB) concentration was 10×10^6 microbubbles ml^{-1}.

pressures above 930 kPa.

For the experiments using the 5 MHz transducer, no displacement was observed for the control experiments. Using a solution of 10×10^6 microbubbles ml^{-1}, higher pressures led to higher displacement of the channel. For the relatively high pressures (above 1,210 kPa), the same displacement pattern where an initial peak displacement was produced, was observed (Fig. **??**(c)).

We evaluated the effect of three different microbubble concentrations and a range of acoustic pressures (Table **??**) for each transducer. Since the results for only two different pressure values were shown in Fig. **??** for each transducer, the effect of pressure on displacements is not clearly depicted. The effect of acoustic pressure and microbubble concentration is shown in Fig. **??** in Section 2C. For each microbubble concentration, the acoustic pressure was increased and the maximum value of the displacement was measured and averaged for 5 consecutive pulses. Higher acoustic pressures produced greater displacements.

For each transducer, data sets for each pressure level were compared for all the microbubble concentrations with ANOVA followed by post-hoc Bonferroni analysis. For the 1 MHz transducer, the results were significantly different between all microbubble concentrations at pressure levels of 355-734 kPa except between 10×10^6 and 20×10^6 microbubbles ml^{-1} solutions. At acoustic pressures of 240 and 300 kPa, the displacements were different except between the control and 4×10^6 microbubbles ml^{-1} and between 10×10^6 and 20×10^6 microbubbles ml^{-1} solutions. For the 3.5 MHz transducer, the results were significantly different between all the microbubble concentrations at pressure levels of 475, 615 and 1395 kPa except between 10×10^6 and 20×10^6 microbubbles ml^{-1} solutions. For the remaining

acoustic pressures, the results were different only between the control and the experiments with microbubbles. Finally, for the 5 MHz transducer, the presence of microbubbles in solutions yielded significantly different displacements compared to the control experiments. At the pressure of 1510 kPa, all the results were found to be significantly different. The resultant displacements from 4×10^6 and 10×10^6 microbubbles ml^{-1} solutions were not found to be significant at pressure levels of 1210, 1810 and 2110 kPa. For each transducer, linear regression was performed on data sets at all pressure levels for each microbubble concentration. All the results were significantly different except for the control experiment with the 3.5 MHz transducer. In addition, slope of the linear fit was found to increase as the microbubble concentration increased for each transducer.

C. Center Frequency

The effect of ultrasound center frequency on the outcome of APP was investigated by keeping the microbubble concentration constant (4×10^6 microbubbles ml^{-1}) and adjusting the acoustic pressure (Fig. **??**(a)). Since each transducer produced a different range of acoustic pressures, the displacement values were calculated as a function of MI. The experiments were repeated using microbubble concentration of 10×10^6 (Fig. **??**(b)) and 20×10^6 microbubbles ml^{-1} (Fig. **??**(c)). For low MI values (below 0.6), no significant difference was observed between the displacement values generated by the transducers for a given MI. We summarized the averaged deformation values of each excitation for all the pressures, center frequencies, microbubble concentrations and control experiments in Fig. **??**. Deformation of the wall was almost constant during excitations with moderate pressures (below

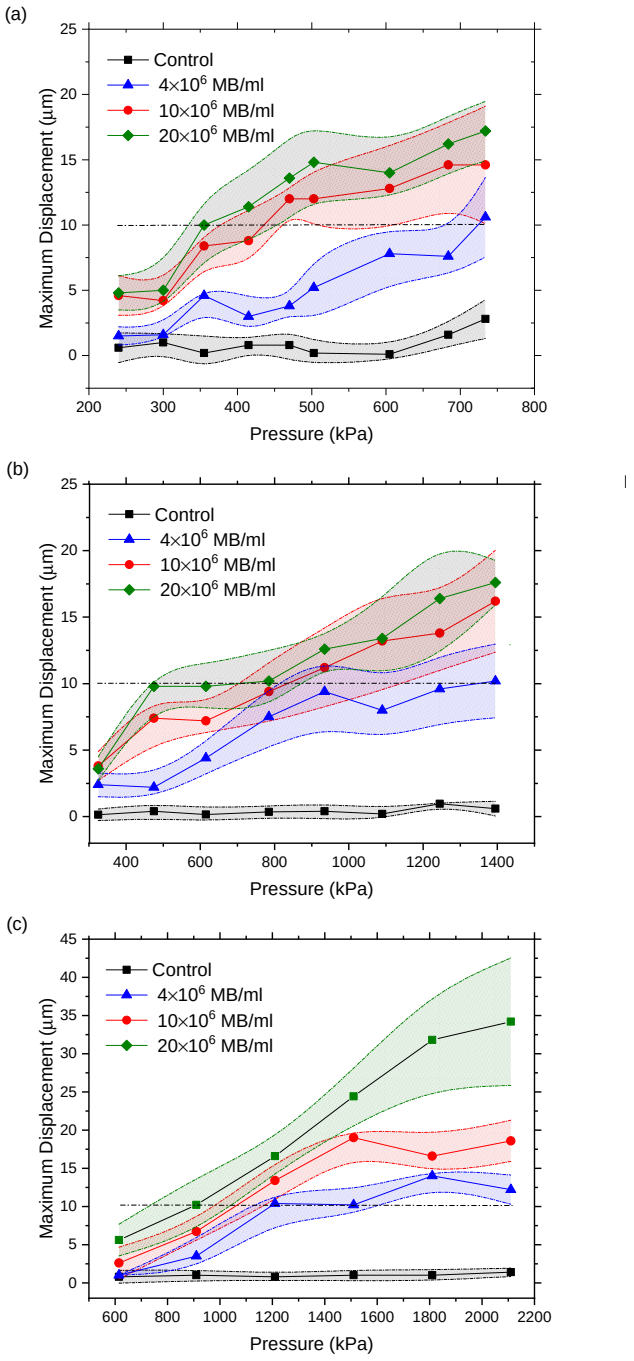

FIG. 4. Maximum displacement over acoustic pressure. The maximum displacement of the wall in each excitation is calculated and then averaged for five consecutive pulses. Values are reported for the experiments (diamonds, circles and triangles) with and (squares) without microbubbles. (a) 1 MHz transducer, (b) 3.5 MHz transducer, (c) 5 MHz transducer. MB: microbubble, Control: without microbubbles. The displacement threshold of 10 μm is shown by the dashed lines.

520 kPa for 1 MHz, 930 kPa for 3.5 MHz, and 1,210 kPa for 5 MHz transducer). However, at higher pressures, the maximum displacement occurred within a few milliseconds and was followed by lower displacements thereafter. Additionally, it was observed that the deformation values did not increase linearly with microbubble concentration or acoustic pressure.

IV. DISCUSSION

We evaluated a range of ultrasound center frequencies, acoustic pressures, and microbubble concentrations that can produce elasticity imaging-relevant deformations using APP. A minimum axial resolution in the orders of tens of microns is required for correlation based tracking techniques according to Cramer-Rao lower band (**??**). The displacement of about 10 μm was observed using 20×10^6 microbubbles ml^{-1} by applying acoustic pressures of 350, 470 and 910 kPa for 1, 3.5 and 5 MHz transducers respectively. Thus APP requires lower acoustic pressures to displace tissue when compared to conventional ultrasound only ARF-based methods (**?**). The magnitude of displacement can be increased by using higher acoustic pressures and microbubble concentrations, which may be necessary for stiffer materials. For soft materials, small detectable displacements are enough for elasticity measurement purposes because the correlation between the pre- and post-compression signals tracked by ultrasound, is reduced for large strains as a result of large displacements.

The displacement was not constant during a single pulse (Fig. **??** and Fig. **??**). At low pressures, the displacement increased slowly. However, at high acoustic pressures, a high displacement was produced in the beginning of the pulse and was followed by a quick de-

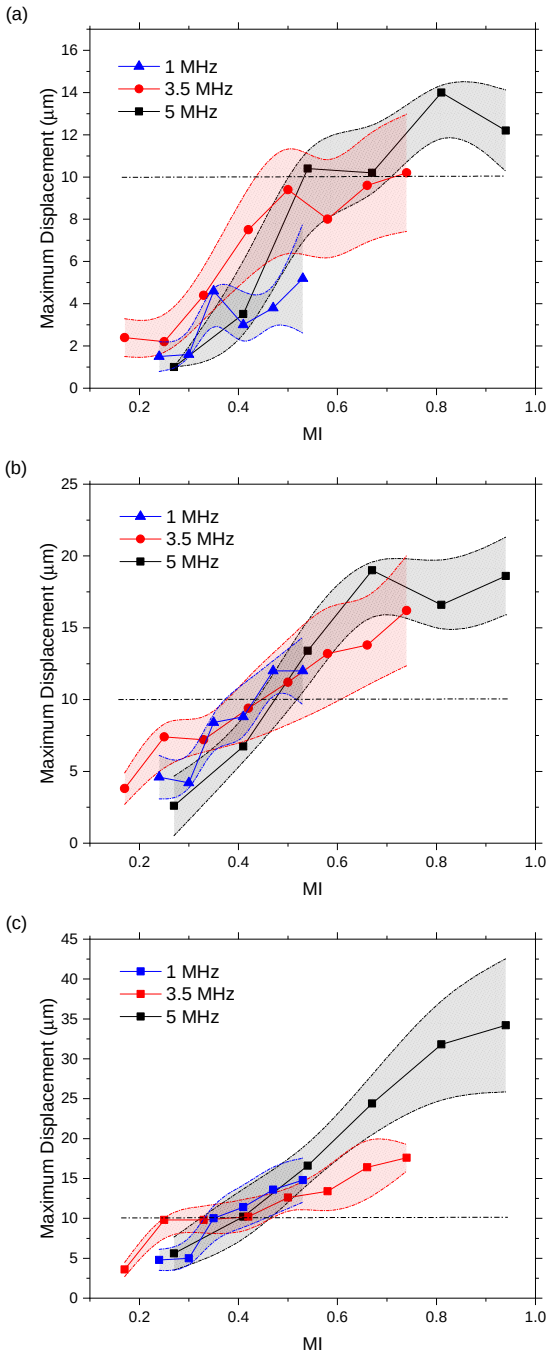

FIG. 5. Maximum displacement over mechanical index (MI). The maximum displacement value in each pulse is averaged for five consecutive pulses. The values are shown for different ultrasound exposure conditions which are center frequencies (squares: 5 MHz, circles: 3.5 MHz and triangles: 1 MHz) and acoustic pressures. The reported displacement values were obtained using microbubble concentrations of (a) 4×10^6 microbubbles ml^{-1}, (b) 10×10^6 microbubbles ml^{-1} (c) 20×10^6 microbubbles ml^{-1}. The displacement threshold of 10 μm is shown by the dashed lines.

crease that stabilized over time. This behavior became more dramatic at higher acoustic pressures and microbubble concentrations. We believe that the sudden decrease of the displacement during an excitation was due to microbubbles being pushed away from the ROE or destroyed within a few microseconds or milliseconds. Previous studies have shown that high acoustic pressures can destroy microbubbles or divide them into smaller particles (**?**). The lower displacement values in the following frames of each pulse could be a result of a subpopulation of microbubbles that have not been destroyed. It should be noted that the microbubble solution was infused into the tunnel at a velocity of 23 mm s^{-1}, which is similar to the blood flow velocity in small arterioles (**??**). The pulse repetition frequency was 200 ms to ensure that unsonicated bubbles replenished the tunnel between consecutive pulses and to establish a constant microbubble concentration for all experiments. However, since the blood velocity depends on the size of the vessel, the effect of flow rate will be considered in future studies.

The amplitude of the deformations could be higher than what was measured in the experiments. The temporal resolution of the camera was limited to 0.83 milliseconds, so the maximum displacement, which could have occurred between frames, may not have been captured. A camera with a higher time resolution is suggested for future work.

For the three center frequencies tested (1, 3.5 and 5 MHz) and with a microbubble concentration of less than 20×10^6 microbubbles $^{-1}$, a displacement of about 10 microns was obtained with mechanical indices lower than 0.4, which is defined as a potential damage threshold (**?**). Since the three center frequencies tested generated almost the same amount of displacements for a given MI (Fig. **??**), different depths of diagnosis can be measured

by the careful selection of center frequencies. For example, using a low center frequency transducer could enable a high depth of elasticity imaging. Although only three center frequencies were tested in this study, other frequencies may be usable. Additionally, it was not possible to determine the optimal center frequency to use, because of the polydispersed size distribution of the microbubbles. The use of more uniformly sized microbubbles could improve the APP-induced deformation magnitude. Future work will include designing microbubbles based on their size and persistence for APP imaging.

Different microbubble concentrations were used to palpate the phantom. In general, higher microbubble concentrations produced greater displacements. However, this rise in displacement with microbubble concentration was not linear. This nonlinear relationship may be due to the translational displacement of bubbles changing as the pushed microbubbles become increasingly dense. In other words, as the microbubbles are displaced towards the distal wall, the separation distance between bubbles reduces (**?**) and secondary radiation forces become greater. Therefore, the force generated by a population of the microbubbles may not equal to sum of the force applied by individual ones.

It was observed that maximum displacement changed sublinearly with MB concentration. As an illustration, maximum displacement values of 0.2, 5.2, 12.8 and 14.8 μm were estimated using no MB (Control), 4×10^6, 10×10^6 and 20×10^6 microbubbles ml^{-1} respectively by applying an acoustic pressure of 503 kPa with the 1 MHz transducer (Fig. **??**(a)). . Results also showed that maximum displacement changes sublinearly with applied pressure. For instance, maximum displacement values of 4.2, 8.4, 12 and 14.5 μm were obtained by applying 300, 355, 470 and 734 kPa respectively, using a 1 MHz transducer and 10×10^6

microbubbles ml^{-1}(Fig. **??**(a)). A mathematical model has been recently proposed to investigate bubble displacement and tissue deformation as a result of a primary Bjerknes force on a fluid-tissue interface (**?**). In the same study, material stiffness dependencies were explored. A similar approach will be considered in a future study to examine the momentum transfer and particle displacement in the presence of the wall for different wall diameter and thickness, as well as for phantoms with different stiffnesses.

V. CONCLUSION

The dependence of APP-induced displacements on acoustic parameters and microbubble concentrations was investigated in this study. Ultrasound-driven microbubbles were shown to apply a force onto a region using lower acoustic pressures than is needed with only ultrasound (control experiment). Deformations at low acoustic pressures and microbubble concentrations were on the order of microns, which is sufficient for elasticity measurements. APP produced elasticity imaging-relevant displacements for different ultrasound center frequencies and was nearly linear with the mechanical index. Since multiple center frequencies could generate enough displacements, elasticity imaging at different diagnosis depths may be possible. APP produced a unique deformation dynamic that varied spatially and temporally since microbubbles moved or were destroyed. The deformation curves varied with acoustic pressure, but was broadly classified into two dynamics: slow rise to a steady state deformation, and rapid high deformation followed by a low steady state deformation. In

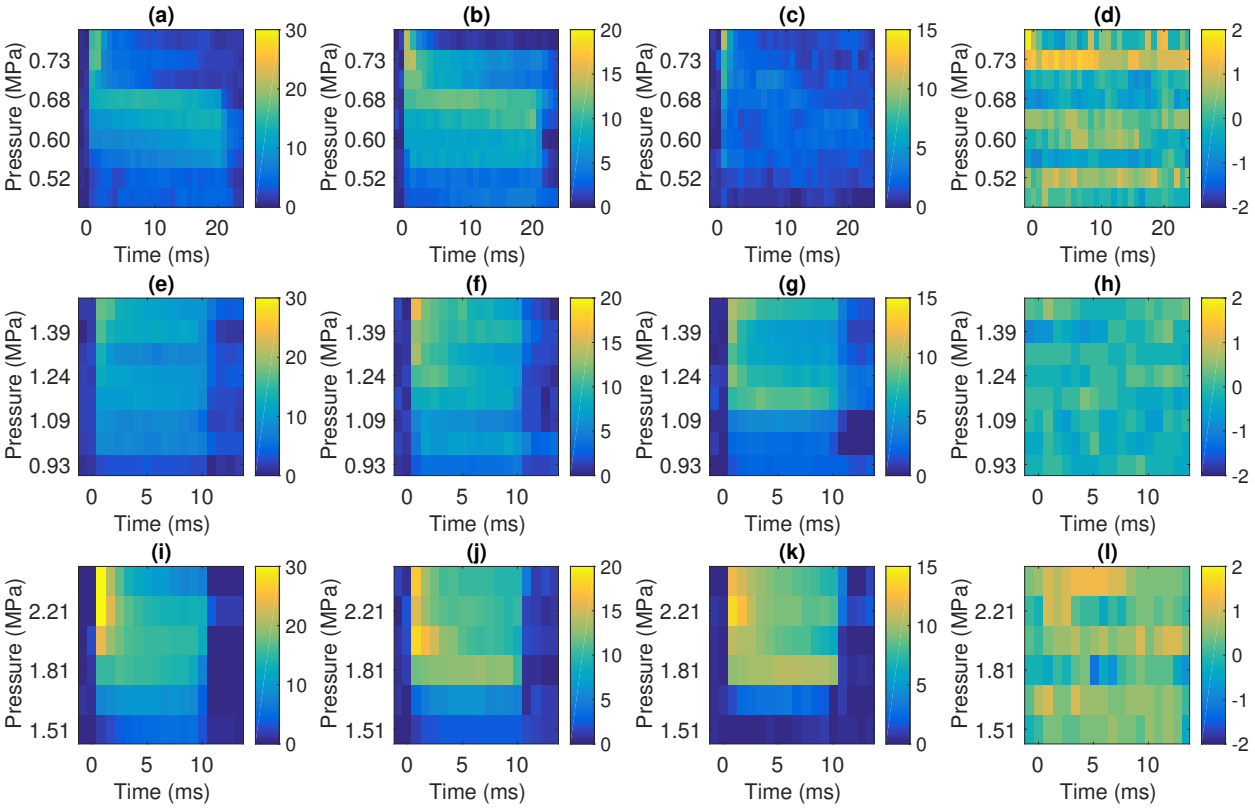

FIG. 6. Mean values of deformations for different acoustic pressures and microbubble concentrations during an excitation for each transducer. (a) 1 MHz transducer, 20×10^6 microbubbles ml^{-1}. (b) 1 MHz transducer, 10×10^6 microbubbles ml^{-1}. (c) 1 MHz transducer, 4×10^6 microbubbles ml^{-1}. (d) 1 MHz transducer, Control. (e) 3.5 MHz transducer, 20×10^6 microbubbles ml^{-1}. (f) 3.5 MHz transducer, 10×10^6 microbubbles ml^{-1}. (g) 3.5 MHz transducer, 4×10^6 microbubbles ml^{-1}. (h) 3.5 MHz transducer, Control. (i) 5 MHz transducer, 20×10^6 microbubbles ml^{-1}. (j) 5 MHz transducer, 10×10^6 microbubbles ml^{-1}. (k) 5 MHz transducer, 4×10^6 microbubbles ml^{-1}. (l) 5 MHz transducer, Control. Control: without microbubbles.

conclusion, APP can produce tissue elasticity imaging relevant deformations using a wide range of acoustic parameters and microbubble concentrations.

ACKNOWLEDGMENTS

This work was supported in part by the Wellcome Trust Institutional Strategic Support Fund to Imperial College London.

[1]She is now with the Department of Biomedical Engineering, Columbia University, New York, NY 10027, USA

[2]Also at: Department of Bioengineering, Imperial College London, London SW7 2BP, United Kingdom

Apfel, R. E. (**1997**). "Sonic effervescence: A tutorial on acoustic cavitation," The Journal of the Acoustical Society of America **101**(3), 1227-1237.

Bouchard, R. R., Dahl, J. J., Hsu, S. J., Palmeri, M. L., and Trahey, G. E. (**2009**). "Image quality, tissue heating, and frame rate trade-offs in acoustic radiation force impulse imaging," IEEE Trans Ultrason Ferroelectr Freq Control **56**(1), 63–76.

Chen, C., Robinson, D., Wilson, L., Griffiths, K., Manoharan, A., and Doust, B. (**1987**). "Clinical sound speed measurement in liver and spleen in vivo," Ultrasonic Imaging **9**(4), 221 – 235.

Chen, E., Novakofski, J., Jenkins, W., and O'Brien, W. (**1996**). "Young's modulus measurements of soft tissues with application to elasticity imaging," IEEE Transactions on Ultrasonics, Ferroelectrics and Frequency Control **43**(1), 191–194.

Chen, H., Brayman, A. A., and Matula, T. J. (**2012**). "Characteristic microvessel relaxation timescales associated with ultrasound-activated microbubbles.," Applied physics letters **101**(16), 163704.

Culjat, M. O., Goldenberg, D., Tewari, P., and Singh, R. S. (**2010**). "A review of tissue substitutes for ultrasound imaging.," Ultrasound in medicine & biology **36**(6), 861–873.

Dalecki, D. (**2007**). "WFUMB Safety Symposium on Echo-Contrast Agents: bioeffects of ultrasound contrast agents in vivo.," Ultrasound in medicine & biology **33**(2), 205–213.

Dayton, P., Morgan, K., Klibanov, A., Brandenburger, G., Nightingale, K., and Ferrara, K. (**1997**). "A preliminary evaluation of the effects of primary and secondary radiation forces on acoustic contrast agents," IEEE Transactions on Ultrasonics, Ferroelectrics and Frequency Control **44**(6), 1264–1277.

Dayton, P. A., Allen, J. S., and Ferrara, K. W. (**2002**). "The magnitude of radiation force on ultrasound contrast agents," The Journal of the Acoustical Society of America **112**(5), 2183–2192.

Doherty, J. R., Trahey, G. E., Nightingale, K. R., and Palmeri, M. L. (**2013**). "Acoustic radiation force elasticity imaging in diagnostic ultrasound.," IEEE transactions on ultrasonics, ferroelectrics, and frequency control **60**(4), 685–701.

Duck, F. A. (**1990**). *Physical Properties Of Tissue: A Comprehensive Reference Book* (Academic Press), pp. 73–165.

Erpelding, T., Hollman, K., and O'Donnell, M. (**2005**). "Bubble-based acoustic radiation force elasticity imaging," IEEE Transactions on Ultrasonics, Ferroelectrics and Frequency Control **52**(6), 971–979.

Fung, Y. C. (**1993**). *Mechanical Properties and Active Remodeling of Blood Vessels* (Springer New York), pp. 321–391.

Fung, Y. C., Zweifach, B. W., and Intaglietta, M. (**1966**). "Elastic environment of the capillary bed.," Circulation research **19**(2), 441–461.

Gefen, A., Gefen, N., Zhu, Q., Raghupathi, R., and Margulies, S. S. (**2003**). "Age-dependent changes in material properties of the brain and braincase of the rat," Journal of Neurotrauma **20**(11), 1163–1177.

Guyton, A. C., and Hall, John E. (John Edward), . (**1996**). *Textbook of medical physiology*, 9th ed ed. (Philadelphia, PA: Saun- ders), pp. 218–220.

Hall, T., Bilgen, M., Insana, M., and Krouskop, T. (**1997**). "Phantom materials for elastography," IEEE Transactions on Ultrasonics, Ferroelectrics and Frequency Control **44**(6), 1355–1365.

Hoskins, P. R. (**2007**). "Physical properties of tissues relevant to arterial ultrasound imaging and blood velocity measurement," Ultrasound in Medicine and Biology **33**(10), 1527 – 1539.

Klabunde, R. E. (**2005**). *Cardiovascular physiology concepts* (Philadelphia, PA: Saunders), pp. 91–93.

Koruk, H., and Choi, J. J. (**2018**). "Displacement of a bubble by acoustic radiation force into a fluid-tissue interface," The Journal of the Acoustical Society of America **143**(4), 2535–2540.

Koruk, H., El Ghamrawy, A., Pouliopoulos, A. N., and Choi, J. J. (**2015**). "Acoustic particle palpation for measuring tissue elasticity," Applied Physics Letters **107**(22), 223701.

412 Krouskop, T. A., Wheeler, T. M., Kallel, F., Garra, B. S., and Hall, T. (**1998**). "Elastic
413 moduli of breast and prostate tissues under compression," Ultrasonic Imaging **20**(4), 260–
414 274.
415 Leighton, T. G., Walton, A. J., and Pickworth, M. J. W. (**1990**). "Primary bjerknes forces,"
416 European Journal of Physics **11**(1), 47-50.
417 Lindner, J. R. (**2004**). "Microbubbles in medical imaging: current applications and future
418 directions," Nat Rev Drug Discov **3**(6), 527–532.
419 McDonald, D. A. (**1974**). *Blood flow in arteries* (Williams & Wilkins, Baltimore, MD),
420 1–496.
421 Neppiras, E. (**1980**). "Acoustic cavitation," Physics Reports **61**(3), 159–251.
422 Nightingale, K. (**2011**). "Acoustic Radiation Force Impulse (ARFI) Imaging: a Review.,"
423 Current medical imaging reviews **7**(4), 328–339.
424 Nightingale, K. R., Palmeri, M. L., Nightingale, R. W., and Trahey, G. E. (**2001**). "On
425 the feasibility of remote palpation using acoustic radiation force," The Journal of the
426 Acoustical Society of America **110**(1), 625–634.
427 Ophir, J., Cspedes, I., Ponnekanti, H., Yazdi, Y., and Li, X. (**1991**). "Elastography: A
428 quantitative method for imaging the elasticity of biological tissues," Ultrasonic Imaging
429 **13**(2), 111 – 134.
430 Parker, K. J., Doyley, M. M., and Rubens, D. J. (**2011**). "Imaging the elastic properties of
431 tissue: the 20 year perspective," Phys Med Biol **56**(1), R1–R29.
432 Pouliopoulos, A. N., Bonaccorsi, S., and Choi, J. J. (**2014**). "Exploiting flow to control the
433 in vitro spatiotemporal distribution of microbubble-seeded acoustic cavitation activity in

ultrasound therapy.," Physics in medicine and biology **59**(22), 6941–6957.

Rooney, J. A., Gammell, P. M., Hestenes, J. D., Chin, H. P., and Blankenhorn, D. H. (**1982**). "Velocity and attenuation of sound in arterial tissues," The Journal of the Acoustical Society of America **71**(2), 462–466.

Sennoga, C. A., Mahue, V., Loughran, J., Casey, J., Seddon, J. M., Tang, M., and Eckersley, R. J. (**2010**). "On sizing and counting of microbubbles using optical microscopy.," Ultrasound in medicine & biology **36**(12), 2093–2096.

Shi, W. T., Forsberg, F., Tornes, A., Østensen, J., and Goldberg, B. B. (**2000**). "Destruction of contrast microbubbles and the association with inertial cavitation," Ultrasound in Medicine & Biology **26**(6), 1009–1019.

Unger, E. C., Porter, T., Culp, W., Labell, R., Matsunaga, T., and Zutshi, R. (**2004**). "Therapeutic applications of lipid-coated microbubbles.," Advanced drug delivery reviews **56**(9), 1291–314.

Varghese, T. (**2009**). "Quasi-Static Ultrasound Elastography.," Ultrasound clinics **4**(3), 323–338.

Walker, W., and Trahey, G. (**1995**). "A fundamental limit on delay estimation using partially correlated speckle signals," IEEE Transactions on Ultrasonics, Ferroelectrics and Frequency Control **42**(2), 301–308.

Woodard, H. Q., and White, D. R. (**1986**). "The composition of body tissues," The British Journal of Radiology **59**(708), 1209–1218.

Yoon, S., Aglyamov, S. R., Karpiouk, A. B., Kim, S., and Emelianov, S. Y. (**2011**). "Estimation of mechanical properties of a viscoelastic medium using a laser-induced microbubble

456 interrogated by an acoustic radiation force.," The Journal of the Acoustical Society of
457 America **130**(4), 2241–2248.
458 Zhang, X., Qiang, B., and Greenleaf, J. (**2011**). "Comparison of the surface wave method
459 and the indentation method for measuring the elasticity of gelatin phantoms of different
460 concentrations.," Ultrasonics **51**(2), 157–164.